PHYSICAL REVIEW LETTERS

# Steady-State Properties of Driven Magnetic Reconnection in 2D Electron Magnetohydrodynamics

L. Chacón,[1] Andrei N. Simakov,[1] and A. Zocco[1,2]

[1]*Theoretical Division, Los Alamos National Laboratory, Los Alamos, New Mexico 87545, USA*
[2]*Burning Plasma Research Group, Department of Energetics, Politecnico di Torino, Torino, Italy*

We formulate a rigorous nonlinear analytical model that describes the dynamics of the diffusion (reconnection) region in driven systems in the context of electron magnetohydrodynamics (EMHD). A steady-state analysis yields allowed geometric configurations and associated reconnection rates. In addition to the well-known open $X$-point geometry, elongated configurations are found possible. The model predictions have been validated numerically with two-dimensional EMHD nonlinear simulations, and are in excellent agreement with previously published work.

Electron physics plays a fundamental role in allowing fast magnetic reconnection in plasmas, both from the kinetic and fluid standpoints [1]. Its role has been linked to the fact that, contrary to the elongated Sweet-Parker geometries found in resistive magnetohydrodynamics (MHD) [2], electron Hall physics is able to maintain an open $X$-point geometry [3–5], thus bypassing the flux-pile-up limitations of resistive MHD. However, recent evidence in the context of open-boundary systems [6] indicates that electron Hall effects can also result in elongated current sheets, thus casting doubt on previous claims, and demanding a more complete explanation of the physics controlling the reconnection region.

In this Letter, we put forth such an explanation. We focus on the electron MHD (EMHD) model [7] as a fundamental element of the more general Hall MHD case, where magnetized electrons decouple from ions and allow fast reconnection to take place (in EMHD, electrons are the only magnetized species). Our approach is similar to that of Sweet and Parker for resistive MHD [2], in that we describe a driven, magnetized plasma around the magnetic diffusion region by a reduced set of time-dependent nonlinear equations, whose steady-state solutions can be found analytically. These solutions are then validated with 2D EMHD simulations of the island coalescence problem (see, e.g., Ref. [8] and references therein). This allows us to gain fundamental insight into the possible geometrical configurations that the dissipation region may adopt, depending on which dissipative mechanism is dominant and on the properties of the driving macroscopic system. In particular, we find that only elongated solutions are possible with resistive dissipation, but that a spectrum of aspect ratios is allowed when electron viscosity is considered. Which configuration is preferred in the latter case depends on the strength of the interaction between macroscopic (driver) and microscopic (reconnection) regions. A stability analysis of the dynamical system with electron viscosity indicates that, when the macroscopic region cannot affect significantly the microscopic dynamics, elon-

gated geometries are preferred. This is consistent with recent work in the context of open-boundary systems [6], where such elongated configurations have been observed.

*Electron MHD model.*—The EMHD model describes magnetized electrons in the presence of a passive, neutralizing ion population. In dimensionless form (using the ion Alfvén speed $v_A$ and the system size $L$ for normalization purposes), it reads [2,7,9]:

$$\partial_t \mathbf{B}^* + \nabla \times (\mathbf{j} \times \mathbf{B}^*) = -\nabla \times \nabla \times (\eta \mathbf{B} - \eta_H \nabla^2 \mathbf{B}),$$

(1)

where $\mathbf{B}^* = \mathbf{B} + d_e^2 \nabla \times \nabla \times \mathbf{B}$, with $d_e = c/\omega_{pe}L$ the electron skin depth, $\omega_{pe}$ the electron plasma frequency, and we have assumed a constant electron density (incompressible electron flow). Here, $\mathbf{B}$ is the magnetic field, $\mathbf{j} = \nabla \times \mathbf{B}$ is the current, $\eta$ is the dimensionless resistivity and $\eta_H$ is the dimensionless electron viscosity (or hyper-resistivity).

In this Letter, we consider the case of $d_e = 0$, which rigorously applies when $d_e \ll \delta \ll d_i = c/\omega_{pi}L$, with $\delta$ the current sheet thickness and $\omega_{pi}$ the ion plasma frequency. This model is of interest to understand the limits that collisional terms place on the reconnection rate in EMHD, and is relevant to previous work [10–12]. The steady-state effects of finite electron inertia have been studied elsewhere [9]. In component form and in 2D geometry (i.e., $\partial_z = 0$), Eq. (1) reads (with $\mathcal{D} = \eta - \eta_H \nabla^2$):

$$\partial_t B_x - \nabla \cdot (\mathbf{j}_p B_x - \mathbf{B}_p j_x) = -\mathcal{D}(\partial_{yx}^2 B_y - \partial_y^2 B_x),$$
$$\partial_t B_y - \nabla \cdot (\mathbf{j}_p B_y - \mathbf{B}_p j_y) = -\mathcal{D}(\partial_{yx}^2 B_x - \partial_x^2 B_y),$$
$$\partial_t B_z - \nabla \cdot (\mathbf{j}_p B_z - \mathbf{B}_p j_z) = \mathcal{D}\nabla^2 B_z.$$

Here, $\mathbf{j}_p = \nabla \times (B_z \mathbf{z})$ and $\mathbf{B}_p = (B_x, B_y)$.

We consider a rectangular 2D reconnection region geometry of dimensions $\delta$ and $w$ (Fig. 1). We define the discrete components of $\mathbf{B}$ as $\tilde{B}_x = B_x(0, \delta/2)$, $\tilde{B}_y = B_y(w/2, 0)$, and $\tilde{B}_z = -B_z(w/2, \delta/2)$. The electron inflow
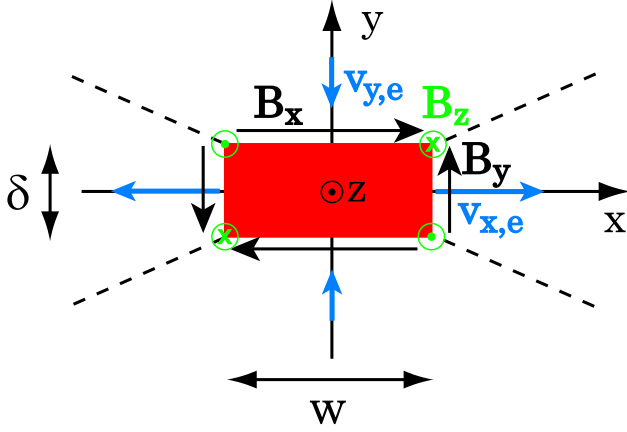
FIG. 1 (color online).   2D reconnection region geometry.

and outflow velocities ($\mathbf{v}_e = -\mathbf{j}_p$) are given as $v_{x,e}(w/2, 0) = 2\tilde{B}_z/\delta$ and $v_{y,e}(0, \delta/2) = -2\tilde{B}_z/w$, respectively. Changing the sign of $\tilde{B}_z$ reverses the flow, so the equations describing the dynamics of discrete quantities in Fig. 1 must be invariant under the substitutions $\tilde{B}_x \leftrightarrow \tilde{B}_y$, $\tilde{B}_y \leftrightarrow \tilde{B}_x$, $\tilde{B}_z \to -\tilde{B}_z$, and $\delta \leftrightarrow w$.

We follow Ref. [13] and use Eq. (1) to obtain time evolution equations for $\tilde{B}_x$, $\tilde{B}_y$, and $\tilde{B}_z$. The equation for $\tilde{B}_x$ is readily obtained by discretizing the $x$ component of Eq. (1) at $(x, y) = (0, \delta/2)$ and using $\partial_x \approx w^{-1}$ and $\partial_y \approx \delta^{-1}$ (which is valid for macroscopically driven systems, but not for spontaneously reconnecting ones, e.g., constant-$\psi$ approximation in tearing mode theory [9,14]). Then, $\partial_t B_x|_{(0,\delta/2)} \to \dot{\tilde{B}}_x - \tilde{B}_x \dot{\delta}/\delta$, where the dot denotes the full time derivative, and the second term in the right-hand side accounts for the boundary motion [13]. Similarly, $\nabla \cdot (\mathbf{j}_p B_x - \mathbf{B}_p j_x) \to \tilde{B}_z \tilde{B}_x/\delta w$ and $-\mathcal{D}(\partial_{yx}^2 B_y - \partial_y^2 B_x) \to D(\tilde{B}_y/\delta w - \tilde{B}_x/\delta^2)$, where $D \equiv \eta + \eta_H(\delta^{-2} + w^{-2})$. The equation for $\tilde{B}_y$ is found from that for $\tilde{B}_x$ by applying the transformation discussed earlier. The equation for $\tilde{B}_z$ is derived by observing that $\mathbf{B}_p \cdot \nabla j_z \to -(\tilde{B}_x/w + \tilde{B}_y/\delta)(\tilde{B}_y/w - \tilde{B}_x/\delta)$ and $\mathbf{j}_p \cdot \nabla B_z = 0$. Thus, our reduced nonlinear dynamical model reads [dropping the tildes and numerical factors of $\mathcal{O}(1)$]:

$$\dot{B}_x - \frac{B_x \dot{\delta}}{\delta} - \frac{B_z B_x}{\delta w} = D\left(\frac{B_y}{\delta w} - \frac{B_x}{\delta^2}\right), \qquad (2)$$

$$\dot{B}_y - \frac{B_y \dot{w}}{w} + \frac{B_z B_y}{\delta w} = D\left(\frac{B_x}{\delta w} - \frac{B_y}{w^2}\right), \qquad (3)$$

$$\dot{B}_z - \frac{B_z \dot{\delta}}{\delta} - \frac{B_z \dot{w}}{w} + \left(\frac{B_x}{w} + \frac{B_y}{\delta}\right)\left(\frac{B_y}{w} - \frac{B_x}{\delta}\right) = -B_z D\left(\frac{1}{\delta^2} + \frac{1}{w^2}\right). \qquad (4)$$

Equations (2)–(4) describe the dynamics of the electron diffusion region. A full dynamical description can be formulated by coupling this model with a macroscopic driver

via the magnetic fields $B_x$ and $B_y$, as is described in Ref. [13] for resistive MHD. Note that the discrete form of the collisional terms in Eqs. (2)–(4) contain sources in addition to sinks. The sinks correspond to dissipation. The sources account for the fact that, at the $X$-point, reconnection of a given magnetic field component results in creation of the orthogonal component (e.g., reconnection of the $B_x$ component will create $B_y$). Capturing these physical sources in the discrete model requires considering $\nabla \times \nabla \times \mathbf{B}$ instead of $-\nabla^2 \mathbf{B}$ in Eq. (1). We note that such discrete collisional terms correctly dissipate the magnetic energy: dotting the collisional terms of Eqs. (2)–(4) by $B_x$, $B_y$, $B_z$, respectively, there results $-D[(B_x/\delta - B_y/w)^2 + B_z^2(\delta^{-2} + w^{-2})] = -D(j_z^2 + j_p^2)$, in agreement with the continuum result.

The steady-state analysis of Eqs. (2)–(4) is of interest to understand intrinsic properties and constraints of reconnection in 2D EMHD. This is so because steady-state solutions also describe evolving systems in regimes where temporal variations are negligible when compared to other terms in the equations, such as at and around the time of maximum reconnection rate [13].

For such an analysis, we define the parameters $b = B_y/B_x$ and $\xi = \delta/w$. Using these, and eliminating $B_z$ from Eqs. (2) and (3) (after setting the time derivatives to zero), one finds $\frac{1}{b} - \xi = \frac{1}{\xi} - b$. This equation has two solution branches, $\xi = b$ and $\xi = b^{-1}$. The latter corresponds to the trivial solution $B_z = 0$, which supports no electron flow, while the nontrivial branch, $\xi = b$ [for which $B_z = D(\xi^{-1} - \xi) \neq 0$] will be central in this Letter. Without loss of generality, we consider $B_z > 0$, which implies $\xi < 1$. Using $\xi = b$ in Eq. (4) and considering the steady state, we obtain

$$(1 + \xi^{-2})[S_\eta^{-1} + S_H^{-1}(1 + \xi^{-2})]^2 = 1, \qquad (5)$$

with $S_\eta \equiv \sqrt{2}B_x/\eta$ and $S_H \equiv \sqrt{2}B_x w^2/\eta_H$. This equation can be solved exactly. However, since the general solution $\xi = \xi(S_\eta, S_H)$ is rather involved, we concentrate next on limiting cases dominated by either resistivity or hyperresistivity.

*Resistive steady state ($\eta \neq 0$, $\eta_H = 0$).*— It reads

$$b = \xi = (S_\eta^2 - 1)^{-1/2} \approx S_\eta^{-1}, \qquad B_z \approx \sqrt{2}B_x, \qquad (6)$$

which predicts that the diffusion region in resistive EMHD is *always* elongated, since $\delta \sim wS_\eta^{-1} \sim w\eta \ll w$ for $S_\eta \gg 1$. Further, it predicts that $B_z \sim B_x$ (in agreement with previous work [3,5,9]), and that $B_y \approx \eta/\sqrt{2}$. Note that $\xi \approx S_\eta^{-1}$ is consistent with the dissipation length scale being set by balancing the whistler wave frequency and the dissipation rate *upstream* of the diffusion region, i.e., $B_x k k_\parallel \sim \eta k^2$, with $k \sim \delta^{-1}$ and $k_\parallel \sim w^{-1}$.

Another interesting result is the reconnection rate $E_z^\eta = \eta j_z$ (the electric field in the ignorable direction at the $X$ point). In our discrete model, $E_z^\eta \approx \eta B_x/\delta$. Using Eq. (6),

we find that $E_z^\eta \approx \sqrt{2}B_x^2/w$; i.e., the reconnection rate is not explicitly dependent on resistivity. This expression (also derived heuristically in Ref. [3]) confirms the possibility of resistivity independent reconnection rates [10–12]. At sufficiently small resistivities, however, this result becomes suspect since associated electron outflows can become arbitrarily large (i.e., $v_{x,e} = B_z/\delta \sim \eta^{-1} \gg v_{A,e} = B_x/d_e$, with $v_{A,e}$ the electron Alfvén speed). A proper treatment requires considering $d_e > 0$ [9].

*Hyper-resistive steady state ($\eta = 0$, $\eta_H \neq 0$).*—The hyper-resistive solution is found similarly, and reads

$$b = \xi = (S_H^{2/3} - 1)^{-1/2} \approx S_H^{-1/3}, \qquad B_z \approx \sqrt{2}B_x. \quad (7)$$

As in the resistive case, $B_z \sim B_x$. However, the aspect ratio of the diffusion region is not a unique function of the dissipation coefficient, and obeys

$$\delta \approx (\eta_H w/\sqrt{2}B_x)^{1/3}. \quad (8)$$

Clearly, instances with either $\delta \sim w \sim (\eta_H/B_x)^{1/2}$ or $\delta \sim (\eta_H/B_x)^{1/3} \ll w \sim 1$ are allowed. This result provides substantial flexibility in the allowed microscopic EMHD configurations. As in resistive EMHD, Eq. (8) is consistent with the dissipation length scale determined by the whistler wave frequency being balanced by the dissipation rate upstream of the diffusion region, i.e., $B_x k k_\parallel \sim \eta_H k^4$.

Which configuration is preferred by the system depends on the nature of the macroscopic driver. In Eqs. (2)–(4), macroscopic feedback is provided by the time derivatives of $B_x$ and $B_y$ (which is how the microscopic region couples with the macroscopic one [13]). A linear stability analysis of Eqs. (2)–(4) (coupled to a macroscopic model), using the equilibria in Eq. (7), would indicate the preferred (stable) configurations. While the full stability analysis is out of the scope of this study, we have performed such an analysis in the limit of a weak macroscopic driver, in which we neglect $\dot{B}_x$ and $\dot{B}_y$, but keep $\dot{\delta}$, $\dot{w}$, and $\dot{B}_z$. The corresponding three linear eigenvalues $\gamma$ are depicted as a function of $\xi$ in Fig. 2 (recall $\xi < 1$ for $B_z > 0$). We find two marginal stability points: one for $\xi = 1$ (which corre-

sponds to static electrons, $B_z = 0$), and another for $\xi \to 0$ (which corresponds to elongated current sheets). This result indicates that, in the absence of a strong interaction with the macroscopic region, and in the presence of electron flow, the diffusion region tends to be elongated. This conclusion supports the recent observation [6] that, for open-boundary systems (which have weak drivers by design, since boundaries allow flux to enter and exit the system as demanded by the microscopic dynamics), the open X-point ($\xi \lesssim 1$) configuration is not stable, and the system evolves towards an elongated configuration ($\xi \ll 1$). Stable open X-point configurations are normally observed for strong macroscopic drivers. However, to study this limit, a suitable macroscopic model (such as that proposed in Ref. [13] for the island coalescence problem) is required to close Eqs. (2)–(4), and this is left for future work.
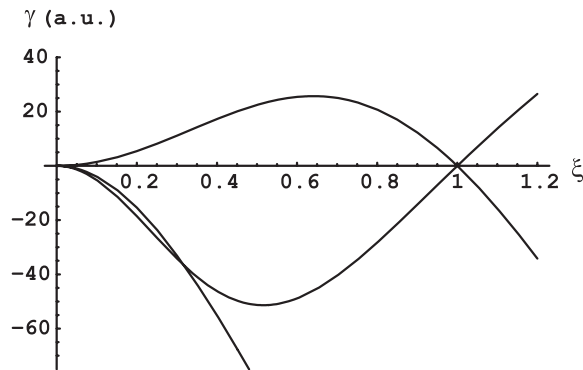
Concerning the hyper-resistive reconnection rate $E_z^H$, we find [using Eq. (8)] $E_z^H = \eta_H \nabla^2 j_z \approx \eta_H(1/\delta^2 + 1/w^2)B_x/\delta \approx \sqrt{2}B_x^2/w$, the same as in resistive EMHD. This result supports earlier claims [15] that the reconnection rate in EMHD may be independent of the dissipation mechanism. In fact, keeping both $\eta, \eta_H \neq 0$, using $E_z = E_z^\eta + E_z^H$, and employing the general solution of Eq. (5), we obtain the reconnection rate $E_z = \sqrt{2}B_x^2(w^2 + \delta^2)^{-1/2}$, which is not explicitly dependent on $\eta$ or $\eta_H$.

*Numerical validation of the EMHD reduced model.*— We validate the reduced model with nonlinear 2D EMHD simulations [16] of the island coalescence problem (as set up in Ref. [8] but with $d_i = c/\omega_{pi}L = 1$). We have measured magnetic fields ($B_x$, $B_y$) and dimensions of the diffusion region ($\delta$, $w$) at the time of maximum reconnection rate ($\delta$ and $B_x$ are measured at half-maximum of the induced current sheet; $w$ and $B_y$ are measured at the point of maximum electron outflow).

We have performed two numerical tests. The first one concerns hyper-resistivity, and tests whether $\delta(\sqrt{2}B_x/w)^{1/3} \approx \eta_H^{1/3}$ [Eq. (8)]. Figure 3 confirms the $\eta_H^{1/3}$ scaling. The second test concerns resistivity. Testing



FIG. 2. Linear eigenvalues $\gamma(\xi)$ for Eqs. (2)–(4) for the steady state in Eq. (7): $\gamma > 0$ indicates instability.
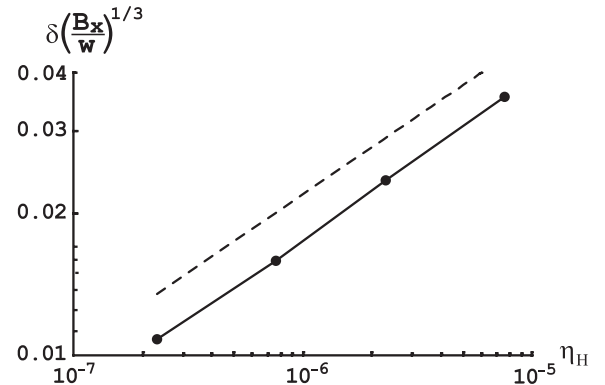


FIG. 3. Scaling of $\delta(B_x/w)^{1/3}$ vs $\eta_H$: numerical 2D EMHD (solid line), $\eta_H^{1/3}$ (dashed line).
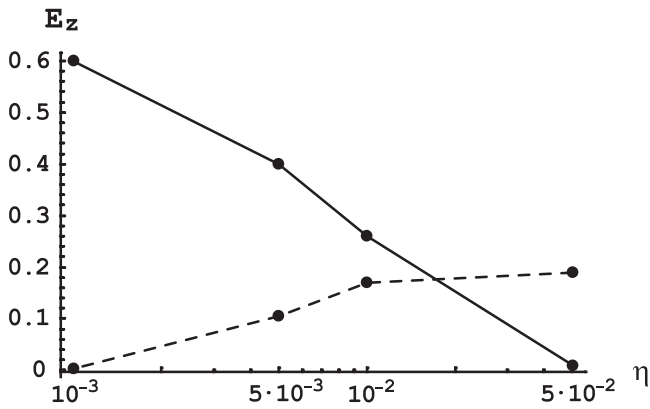
FIG. 4.   Reconnection rates due to resistivity ($E_z^{\eta}$, dashed line) and hyper-resistivity ($E_z^H$, solid line).

the resistive regime directly becomes computationally difficult even for moderate resistivities due to the resolution requirements of $\delta \sim \eta$, and the numerical requirement of higher-order dissipation [1]. Instead, we consider both finite $\eta$ and $\eta_H$, and we aim at validating the value of $\eta$ at which the resistive regime transitions to a hyper-resistive one. The transitional $\eta$ is defined such that both dissipation mechanisms contribute equally to the reconnection rate, yielding $\eta_t \approx \eta_H(1/w^2 + 1/\delta^2) \approx (\sqrt{2}B_x/w)^{2/3}\eta_H^{1/3}$. For $\eta_H = 7.63 \times 10^{-7}$, 2D EMHD simulations give $B_x \approx 0.1$ and $w \approx 0.05$ for the range of $\eta$ considered, and, therefore, $\eta_t \approx 1.8 \times 10^{-2}$. Numerical values of $E_z^{\eta}$ and $E_z^H$ vs $\eta$ are depicted in Fig. 4, and confirm the predicted $\eta_t$. Note that large-$\eta$ results in Fig. 4 are still in the asymptotic regime, since $\delta \sim \eta w/B_x \approx 0.025 \ll 1$ for $\eta \sim 0.05$. Additional numerical confirmation of the theoretical results on the properties of the reconnection region proposed in this Letter can be found in Ref. [17].

In conclusion, we have derived a rigorous reduced nonlinear analytical model of the reconnection region within the context of 2D EMHD. In steady state, we find that the shape of the region depends on the dissipation mechanism and the external driver. For resistivity-dominated regimes, the dissipation region is always elongated in the direction of outgoing electron flow. For electron viscosity ones, various aspect ratios of this region are possible depending on the external driver, and elongated configurations are preferred for weak drivers. Independently of the dissipation mechanism and the driver, the reconnection rate is not explicitly dependent on the dissipation coefficients. Our model has been successfully benchmarked with full 2D EMHD numerical simulations and can be used as a benchmark for future numerical simulation tools.

[1] J. Birn, J. F. Drake, M. A. Shay, B. N. Rogers, R. E. Denton, M. Hesse, M. M. Kuznetsova, Z. W. Ma, A. Bhattacharjee, and A. Otto *et al.*, J. Geophys. Res. **106**, 3715 (2001).

[2] D. Biskamp, *Magnetic Reconnection in Plasmas* (Cambridge University Press, Cambridge, England, 2000).

[3] M. A. Shay, J. F. Drake, B. N. Rogers, and R. E. Denton, Geophys. Res. Lett. **26**, 2163 (1999).

[4] B. N. Rogers, R. E. Denton, J. F. Drake, and M. A. Shay, Phys. Rev. Lett. **87**, 195004 (2001).

[5] M. A. Shay, J. F. Drake, M. Swisdak, and B. N. Rogers, Phys. Plasmas **11**, 2199 (2004).

[6] W. Daughton, J. Scudder, and H. Karimabadi, Phys. Plasmas **13**, 072101 (2006).

[7] A. S. Kingsep, K. V. Chukbar, and V. V. Yan'kov, *Reviews of Plasma Physics* (Consultants Bureau, New York, 1990), Vol. 16, p. 243.

[8] D. A. Knoll and L. Chacón, Phys. Rev. Lett. **96**, 135001 (2006).

[9] S. V. Bulanov, F. Pegoraro, and A. S. Sakharov, Phys. Fluids B **4**, 2499 (1992).

[10] Z. W. Ma and A. Bhattacharjee, Geophys. Res. Lett. **23**, 1673 (1996).

[11] X. Wang, A. Bhattacharjee, and Z. W. Ma, J. Geophys. Res. **105**, 27 633 (2000).

[12] J. C. Dorelli and J. Birn, Phys. Plasmas **8**, 4010 (2001).

[13] A. N. Simakov, L. Chacón, and D. A. Knoll, Phys. Plasmas **13**, 082103 (2006).

[14] N. Attico, F. Califano, and F. Pegoraro, Phys. Plasmas **7**, 2381 (2000).

[15] M. A. Shay and J. F. Drake, Geophys. Res. Lett. **25**, 3759 (1998).

[16] L. Chacón and D. A. Knoll, J. Comput. Phys. **188**, 573 (2003).

[17] V. Lukin, Ph.D. thesis, Princeton University, 2007.